DIU Journal of Science and Technology Volume 12, Issue 1, January 2017

2017-01

First-Principles Study of Structural, Electronic and Optical Properties of Lead-Free Organic Inorganic Tin Halide Perovskites for Photovoltaic Applications

Shalauddin

Daffodil International University

FIRST-PRINCIPLES STUDY OF STRUCTURAL, ELECTRONIC AND OPTICAL PROPERTIES OF LEAD-FREE ORGANIC INORGANIC TIN HALIDE PEROVSKITES FOR PHOTOVOLTAIC APPLICATIONS

Shalauddin
Department of General Educational Development
Daffodil International University, Bangladesh
Email: shalauddin.ns@diu.edu.bd

Abstract: *Promising candidates in this respect are organometal perovskites ABX_3, which have been intensely investigated during the last years. In this work, we have calculated the geometry optimization, band structure, optical properties and carrier mobility for tetragonal phase of non-toxic perovskite halide $CH_3NH_3SnCl_3$ and $CH_3NH_3SnI_3$ by applying density functional theory (DFT) with the generalized gradient approximation (GGA) correlation of Perdew-Berke-Erzndof (PBE). The results have showed that $CH_3NH_3SnCl_3$and $CH_3NH_3SnI_3$ have good optical absorption coefficient, which can be a good application for solar light harvester.*

Keywords: *First-Principles Study, Perovskites solar cell, Solar cell, Structural, Electronic and Optical Properties of Perovskites solar cell.*

1. Introduction

Perovskites generally refer to a class of oxides with chemical formula ABX_3 that exhibit sought-after physical properties such as magnetic, ferroelectric, and two-dimensional electronic conductivity [1,2]. This is due to the high efficiency of solid-state solar cells based on halide perovskite, which reached 22.1% in 2016 [3], 17.9% in 2014 [4], up from 9.7% in 2012 [5]. For comparison, liquid DSCs electrolyte solar cells had an efficiency of 3.8%in 2009 [6]. In the past 3 years, photovoltaics were found lack of considerable and promising research on hybrid halide perovskite materials. Their potential applications included solar-cell absorbers [7,9], topological insulators [10], and superconductors [11]. Methyl-ammonium metal-halide, with similar structure of ABX_3 (A=organic molecules, B=metal, X=halide) existing in nature, revealed one of a potential material available for next-gen solar cell fabrications [12,13].

In this framework, the comprehension of the correlations between structure, chemical composition, and properties through first-principles calculations can give the possibility of designing new functional structures, with desired physical properties. The $CH_3NH_3BX_3$ compounds are a subclass of the ABX_3 family, with cubic structures where the organic component is included in the extended three-dimensional inorganic cage. The negative charge is typically localized on the halide atoms and the CH_3NH_3+ cation occupies the center of the cubic cell. In these structures, the divalent metal '*B*' is in octahedral coordination with halogen atoms forming classical perovskiticoctahedra.

At high temperature, CH_3NH_3+ is free to rotate because the potential barriers between the different stable configurations are smaller than the thermal energy and so all these compounds own a high temperature cubic phase. This is confirmed by the experimental [14] findings demonstrating, on the basis of nuclear magnetic resonance and nuclear quadrupole resonance, that CH_3NH_3+ cations undergo rapid isotropic reorientation at room temperature in the CH_3NH_3Pb*X*$_3$ (*X*=Cl, I) lead compounds. A similar behavior is found [15,16] in isostructural compounds such as tin (II) halide CH_3NH_3Sn*X*$_3$ compounds.

Previous studies [15] on CH_3NH_3Sn*X*$_3$ showed that, in this class of compounds, transport properties seem to evolve from metallicity to semi conductivity along the series I→Br→Cl. Our main goal was to discover and target the low cost,

Date of submission : 09.10.2016 Date of acceptance : 14.01.2017

efficient, flexible and durable photovoltaics for thin film fabrications, in exploring the plethora of producing clean and sustainable energy. In providing an excellent bandgap and charge mobility, tin iodide were suitable candidates for light-absorbing purposes. In this work, absorption analysis, room temperature resistivity, and x-ray structural analysis on $CH_3NH_3SnX_3$ thin films (with *X*=Cl, I) are combined with *ab initio* calculations.

2. Computational Methods

This work involved with the calculation of single point energy, geometry optimization, band structure, using the Kohn-Sham DFT calculation. The total energy of the electron system was calculated with the energy-cutoff of 240eV and k-point grid of 2×2×2, under Monkhorst Pack special integration scheme, with brillouin sampling of 7 points. For band structure calculation, the total energy SCF tolerance was placed to a value of 2×10^{6} eV/atom, with the maximum force of 0.05eV/Å, displacement of of 0.002Å and maximum stress of 0.1GPa. The interaction of the valence core was provided, with the norm-conserving pseudopotential, under Martin-Troullier scheme, other than ultrasoftscheme, in evaluation of optical material properties, where the electron orbitals of, $2s^2\ 2p^2$ for C atom, $2s^2\ 2p^3$ for N atom, $5s^2\ 5p^2$ for Sn atom and $5s^2\ 5p^5$ for I atom were chosen.

For band structure calculation, the separation space of 0.025 $Å^{-1}$ and 12 empty bands at k point separation were employed. Here, the description of the Generalized gradient approximation (GGA) of Perdew-Berke-Erzndof (PBE) were treated when applying the exchange-correlation method. The crystal structure optimization and electronic structure calculations of halide perovskites ABX_3 were performed by using the Cambridge Sequential Total Energy Package (CASTEP).

3. Results and Discussions

As representative of ABX_3 (A=CH_3NH_3; B=Sn; X=Cl, I) crystallizes in the perovskite structure, which are respectively shown in Figure 1.1(a) and 1.1(b). The structure belongs to the tetragonal space groups 4/mmm. B is a metal bonded to six X anions, and BX_6octahedra are corner-connected to form a three-dimensional framework.

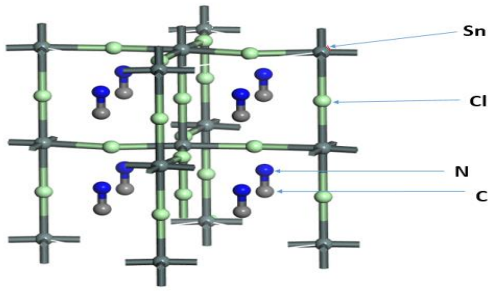

Figure 1.1(a): Structure of $CH_3NH_3SnCl_3$

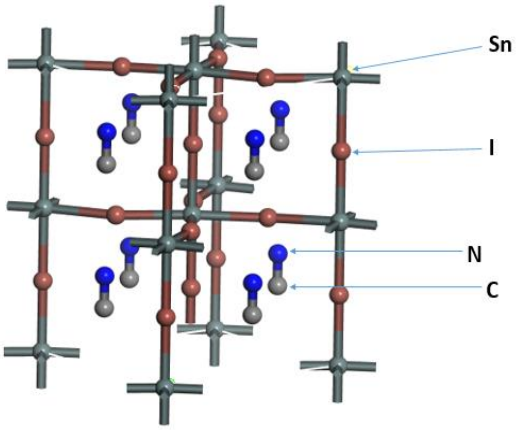

1.

Figure 1(b): Structure of $CH_3NH_3SnI_3$.

Figure 1.2(a) Band structure of $CH_3NH_3SnCl_3$ and 1.2 (b) band structure of $CH_3NH_3SnI_3$ obtained using PBE method.

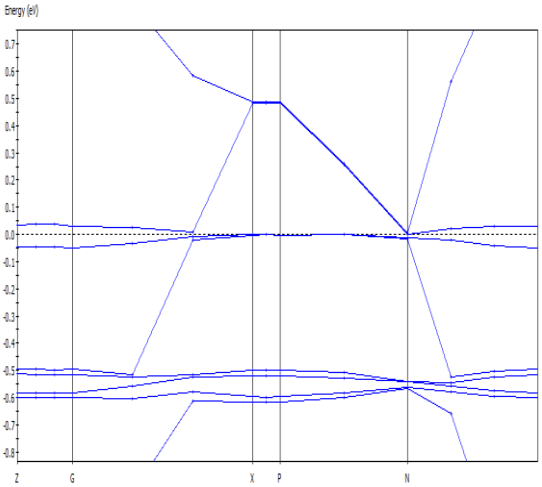

Figure 1.2(a): Band structure of $CH_3NH_3SnCl_3$.

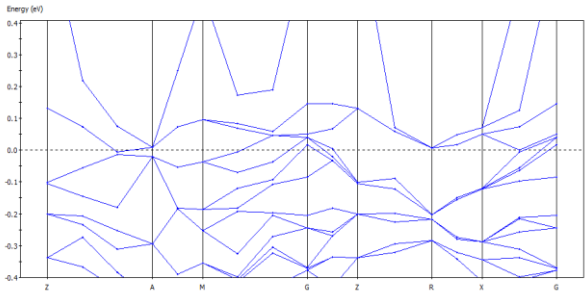

Figure 1.2(b): Band structure of $CH_3NH_3SnI_3$

The calculations of the electronic band structure help one to understand the shape of the Fermi surface. The material properties can be understood if one can identify the character of dominant bands near the Fermi level, their energy etc. In this way knowledge of the electronic band structure provides predictive insight and understanding of certain very important properties of solids. The band structures of $CH_3NH_3SnCl_3$ and $CH_3NH_3SnI_3$ are depicted in Figure 1.2(a) and 1.2(b). The results show that the conduction bands minimum (CBM) and the valence bands maximum (VBM) are at R (1.0, 0.0, 0.0) symmetry point in the Brillouin zone.

From Table 1.1: we can also notice that the band gaps of $CH_3NH_3SnCl_3$ is larger. The reason for this is origin of valence band maximum (VBM) and conduction band minimum (CBM).
Hence, these ABX_3 perovskites in tetragonal phase $CH_3NH_3SnCl_3$ have direct band-gap nature at R symmetry point.
The lattice constants and band gaps of $CH_3NH_3BX_3$ obtained by using both PBE methods are listed in Table 1.1**Error! Reference source not found.**
The calculated lattice constants of $CH_3NH_3SnI_3$ by PBE are in good agreement with experimental values as indicated in Table 1.1**Error! Reference source not found.**
The lattice constant increases from Cl to I. The reason for this is simply due to the larger atom of I atom than that of Sn atom or Cl atom.

Table 1.1 Lattice constants and bandgap of ABX_3 using both PBE method.

ABX_3	Lattice Constants (Å)		Bandgap (eV)	
	PBE	**Experimental value**	**PBE**	**Experimental value**
$CH_3NH_3SnCl_3$	16.885	5.76 [27]	0.002	2.18 [28]
	-	-		
$CH_3NH_3SnI_3$	a = b = 8.594	8.727[29]	0.0	1.30 [30]
	c = 12.664	12.502 [29]		

The bandgap calculated by the PBE methods without considering the spin orbit coupling (SOC) are not consistent with the calculated value.

We find that $CH_3NH_3SnCl_3$ has a direct bandgap which is consistent with experimental result but the value is too poor. On the other hand $CH_3NH_3SnI_3$ has overlapped bandgap but the experimental value is 1.30 eV as given in the Table 1.1**Error! Reference source not found.**The density of states (DOS) of a system describes the number of states per interval of energy at each energy level that are available to be occupied. A DOS of zero means that no states can be occupied at that energy level.

The total density of states for $CH_3NH_3SnCl_3$ and $CH_3NH_3SnI_3$ calculated using PBE method is shown in 1.3.

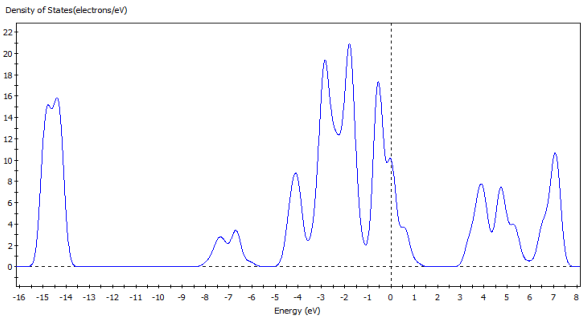

a. Graph of reflectivity-wavelength

b. Graph of reflectivity-wavelength

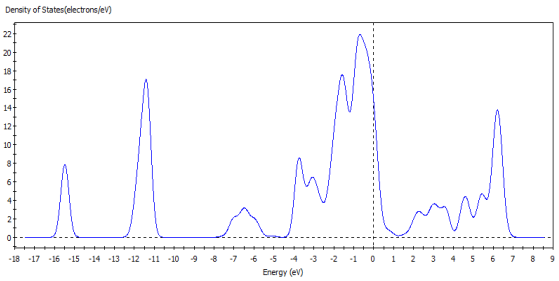

Figure 1.3: Total DOS of (a) $CH_3NH_3SnCl_3$ and (b) $CH_3NH_3SnI_3$.

Table 1.2 Bond distances between Sn-Cl and Sn-I of $CH_3NH_3SnCl_3$ and $CH_3NH_3SnI_3$ obtained by using PBE methods.

ABX_3	**Bonds**	**Bond Length (Å)**
$CH_3NH_3SnCl_3$	Cl 2 - Sn 2	1.189
	Cl 6 - Sn 2	2.677
$CH_3NH_3SnI_3$	I 2 - Sn 2	3.060
	I 6 - Sn 2	3.230

The ABX_3 compounds have a similar energy distribution of the eigenstates. It is observed that the VBM of $CH_3NH_3SnI_3$ is lower than $CH_3NH_3SnCl_3$, and the CBM of $CH_3NH_3SnCl_3$ is higher than $CH_3NH_3SnI_3$, leading to a larger band gap of $CH_3NH_3SnCl_3$. The higher VBM of $CH_3NH_3SnCl_3$ is due to the stronger Sn s–Cl p* antibonding interaction because of a small bond length of Sn–Cl as shown in Table. As for the CBM, the Sn p–I p* orbital is higher than Sn p–Cl p* orbital because the atomic orbital energy of I p is higher than the energy of Sn p. Therefore, the energy gap of $CH_3NH_3SnCl_3$ is wider than $CH_3NH_3SnI_3$.

c. Graph of absorption wavelength.

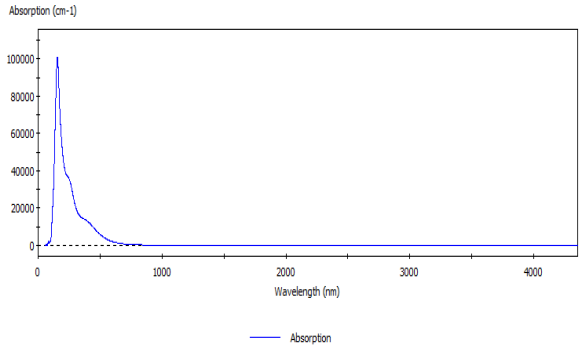

(a)

c. Graph of conductivity-wavelength.

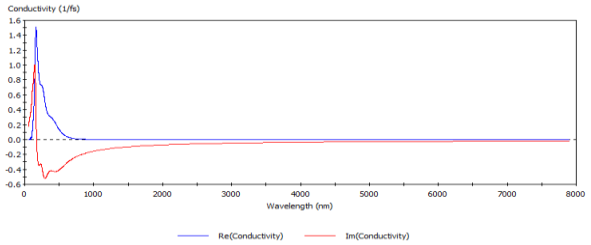

(b)

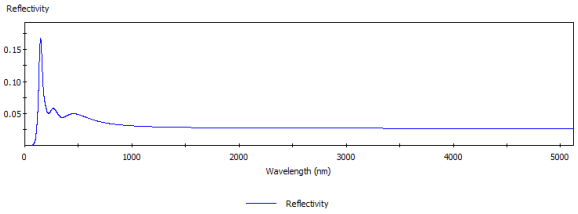

(c)

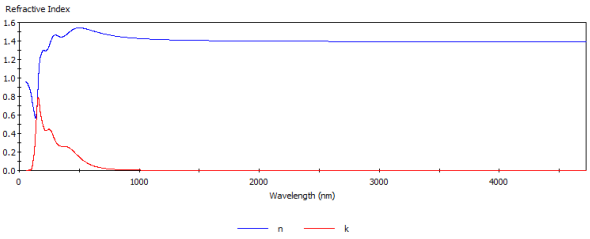

(d)

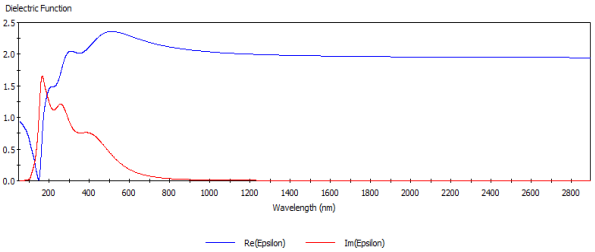

(e)

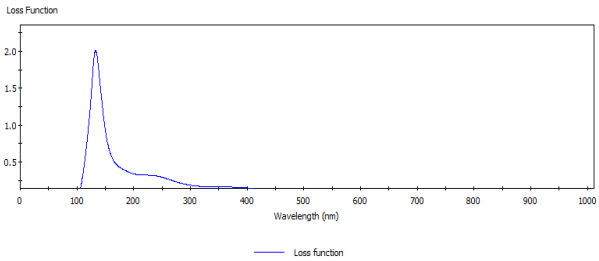

(f)

Figure 1.4: (a), (b) (c), (d), (e) and (f) Diagram illustrating the optical properties of $CH_3NH_3SnCl_3$ at bulk, with scissors operator = 0 eV, instrumental smearing of 0.5eV, polarized, the polarization in direction of (1.0, 0.0, 0.0).

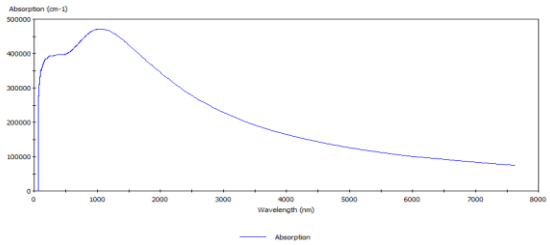

(a)

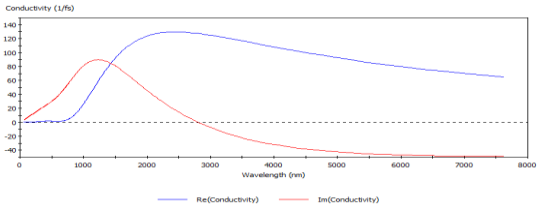

(b)

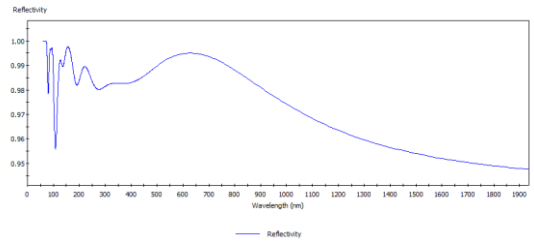

(c)

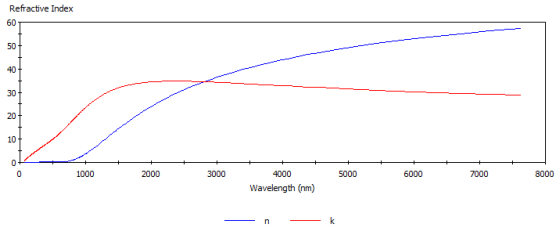

(d)

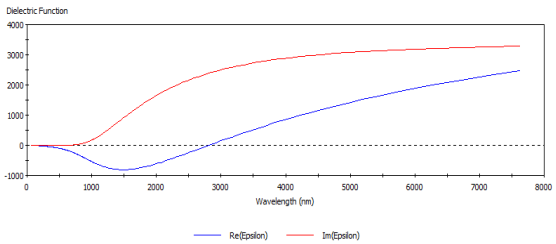

(e)

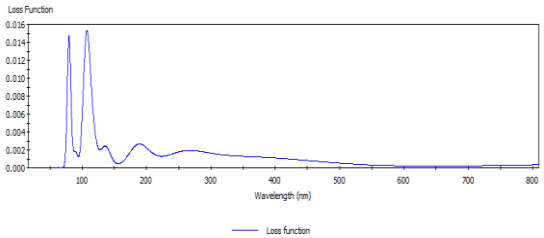

(f)

Figure 1.5: (a), (b), (c), (d), (e) and (f) Diagram illustrating the optical properties of $CH_3NH_3SnI_3$ at bulk, with scissors operator = 0 eV, instrumental smearing of 0.5eV, polarized, the polarization in direction of (1.0, 0.0, 0.0).

Optical properties are important in solid state physics because the study of the optical functions of solids provides a better understanding of the electronic structure.$CH_3NH_3SnCl_3$ and $CH_3NH_3SnI_3$ have the excellent ability of light absorption in the visible zone. The optical absorption coefficients of the tetragonal phase are shown in

Figure 1.4 and Figure 1.5. We focus on the optical properties and the absorption coefficient curve. From figure, it is clearly that the $CH_3NH_3SnCl_3$ has the more superior absorption performance than that of $CH_3NH_3SnI_3$. For $CH_3NH_3SnCl_3$, the optical absorption found was indicating its peak ranges from 145 nm to 700 nm and have a peak at 320 nm near to the visible light spectrum. Thus, $CH_3NH_3SnCl_3$ can absorb light in the visible range.

For $CH_3NH_3SnI_3$, the absorption coefficient curve move from violet spectrum to the red spectrum exhibiting red shift phenomenon and have a peak near to the visible light spectrum. The optical conductivity of the $CH_3NH_3SnCl_3$ has a greater value than $CH_3NH_3SnI_3$with respect to increasing wavelength as shown in Fig. The reflectivity of each perovskite increase**s** with increasing wavelength. The reflectivity spectrum shows that the materials are reflector within the wavelength range 150-950 nm for $CH_3NH_3SnI_3$, 120-200 nm for $CH_3NH_3SnCl_3$. In the energy-loss spectrums, the first peaks are found at 140nm for $CH_3NH_3SnCl_3$ and 110nm for $CH_3NH_3SnI_3$. This indicates to a rapid reduction in the reflectance. It is seen that the real part of the dielectric function vanishes at about 7900 nm for each perovskite. The refractive index of $CH_3NH_3SnCl_3$is found to have the values 500nm and of $CH_3NH_3SnI_3$ is 7500 nm.

The absorption of the $CH_3NH_3SnCl_3$ and $CH_3NH_3SnI_3$ is significantly intensive, which indicate that $CH_3NH_3SnCl_3$ and $CH_3NH_3SnI_3$ have superiority in utilizing solar energy.

4. Conclusion

In our calculation, the electronic structures of ABX_3 are systematically studied by first-principles calculations using PBE approximations. We compare PBE results to experimental data for the band gap and our calculated results of band gap deviated from the experimental value. The CBM of ABX_3 larger for $CH_3NH_3SnCl_3$, while the VBM of ABX_3 are more complicated, depending on both the bond length of B–X. The calculations at this level of approximation were only considered as a first approximation and had limited value as a quantitative prediction. The optical absorption found was indicating its peak near to the visible light spectrum. This will be useful in converting the sun radiation to electrical or heat energy, which will turn out to be beneficial in fabrication of photovoltaic absorbers, in providing a clean, environmentally-friendly renewable energy resource. The valence band maximum (VBM) is mainly the contribution of the p orbitals of the Cl atom and partly the contribution of the s orbital of Sn, while the p orbitals of the Sn mainly contribute to the conduction band minimum (CBM). The light absorption coefficient shows that the $CH_3NH_3SnCl_3$ exhibits the strongest absorption performance, which consist in the same ordering of the band gap change. Although in our observed results are poor, the bandgap, optical properties of $CH_3NH_3SnCl_3$ lag behind CH3NH3PbI3, we can improve performances through more iterations and considering others parameters like Heyd–Scuseria–Ernzerhof (HSE) hybrid functional, spin orbit coupling (SOC), GW many-body corrections. Therefore, my next work will be to improve the optical coefficient of $CH_3NH_3SnCl_3$ and $CH_3NH_3SnI_3$.

References

[1] R. E. Cohen, "No Title," *Nature*, vol. 358, pp. 136–138, 1992.

[2] M. and J. L. G. F. A.Pena, "No Title," *Chem. Rev.*, vol. 101, pp. 1981–2017, 2001.

[3] "Best Research-Cell Efficiencies, www.nrel.gov/ncpv/images/efficiency_chart. jpg (accessed: April 2016)." .

[4] "http://www.nrel.gov/ncpv/images/efficiency_chart.jpg."

[5] H.-S. Kim, C.-R. Lee, J.-H. Im, K.-B. Lee, T. Moehl, A. Marchioro, M. G. S.-J. Moon, R. Humphry-Baker, J.-H. Yum, J. E. Moser, and 35 and N.-G. Park, "No Title," *Sci. Rep.*, vol. 2, p. 591, 2012.

[6] Y. S. and T. M. A. Kojima, K. Teshima, "No Title," *J. Am. Chem. Soc.*, vol. 131, 2009.

[7] I. Chung, B. Lee, J. He, R. P. H. Chang, and M. G. Kanatzidis, "All-solid-state dye-sensitized solar cells with high efficiency.," *Nature*, vol. 485, no. 7399, pp. 486–9, 2012.

[8] J. Burschka, N. Pellet, S.-J. Moon, R. Humphry-Baker, P. Gao, M. K. Nazeeruddin, and M. Grätzel, "Sequential deposition as a route to high-performance perovskite-sensitized solar cells.," *Nature*, vol. 499, no. 7458, pp. 316–320, 2013.

[9] and T. M. Akihiro Kojima,† Kenjiro Teshima,‡ Yasuo Shirai, "Organometal Halide Perovskites as Visible-Light Sensitizers for Photovoltaic Cells," *J Am Chem Soc*, vol. 131, no. October, pp. 6050–6051, 2009.

[10] T. Baugher, a. Gade, R. Janssens, S. Lenzi, D. Bazin, B. Brown, M. Carpenter, a. Deacon, S. Freeman, T. Glasmacher, G. Grinyer, F. Kondev, S. McDaniel, "Erratum: Intermediate-energy Coulomb excitation of ^{58,60,62}Cr: The onset of collectivity toward N=40 [Phys. Rev. C 86, 011305(R) (2012)]," *Phys. Rev. C*, vol. 86, no. 4, p. 011305, 2012.

[11] Y. Takahashi, R. Obara, Z.-Z. Lin, Y. Takahashi, T. Naito, T. Inabe, S. Ishibashi, and K. Terakura, "Charge-transport in tin-iodide perovskite CH3NH3SnI3: origin of high conductivity.," *Dalt. Trans.*, vol. 40, no. 20, pp. 5563–5568, 2011.

[12] L. Lang, J.-H. Yang, H.-R. Liu, H. J. Xiang, and X. G. Gong, "First-principles study on the electronic and optical properties of cubic ABX 3 halide perovskites," *Phys. Lett. A*, vol. 378, pp. 290–293, 2014.

[13] P. Umari, E. Mosconi, and F. De Angelis, "Relativistic GW calculations on CH3NH3PbI3 and CH3NH3SnI3 perovskites for solar cell applications.," *Sci. Rep.*, vol. 4, p. 4467, 2014.

[14] O. Knop, R. E. Wasylishen, M. A. White, T. S. Cameron, and M. J. M. Van Oort, "Alkylammonium lead halides. Part 2. CH 3 NH 3 PbX 3 (X = Cl, Br, I) perovskites: cuboctahedral halide cages with isotropic cation reorientation," *Can. J. Chem.*, vol. 68, no. 3, pp. 412–422, 1990.

[15] K. Yamada, H. Kawaguchi, T. Matsui, T. Okuda, and S. Ichiba, "Structural Phase Transition and Electrical Conductivity of the Perovskite CH3NH3Sn1-xPbxBr3 and CsSnBr3.pdf," *Bull. Chem. Soc. Jpn.*, no. 63. pp. 2521–2525, 1990.

[16] N. Onoda-Yamamuro, O. Yamamuro, T. Matsuo, H. Suga, N. Tsuchiya, T. Kamiyama, and H. Asano, "Neutron-diffraction study of CD3ND3SnBr3: Semiconductor-insulator transition with orientational ordering," *Phys. B Phys. Condens. Matter*, vol. 213–214, no. C, pp. 411–413, 1995.